1

Quantum Theory of Thermoelectric Power (Seebeck Coefficient)

Shigeji Fujita[1] and Akira Suzuki[2]
[1]*Department of Physics, University at Buffalo, SUNY, Buffalo, NY*
[2]*Department of Physics, Faculty of Science, Tokyo University of Science, Shinjyuku-ku, Tokyo*
[1]*USA*
[2]*Japan*

1. Introduction

When a metallic bar is subjected to a voltage (V) or a temperature (T) difference, an electric current is generated. For small voltage and temperature gradients we may assume a linear relation between the electric current density $\boldsymbol{j}$ and the gradients:

$$\boldsymbol{j} = \sigma(-\boldsymbol{\nabla} V) + A(-\boldsymbol{\nabla} T) = \sigma \boldsymbol{E} - A\boldsymbol{\nabla} T, \tag{1.1}$$

where $\boldsymbol{E} \equiv -\boldsymbol{\nabla} V$ is the electric field and σ the conductivity. If the ends of the conducting bar are maintained at different temperatures, no electric current flows. Thus from Eq. (1.1), we obtain

$$\sigma \boldsymbol{E}_S - A\boldsymbol{\nabla} T = 0, \tag{1.2}$$

where $\boldsymbol{E}_{\rm S}$ is the field generated by the thermal electromotive force (emf). The *Seebeck coefficient (thermoelectric power)* S is defined through

$$\boldsymbol{E}_{\rm S} = S\boldsymbol{\nabla} T, \quad S \equiv A/\sigma. \tag{1.3}$$

The conductivity σ is positive, but the Seebeck coefficient S can be positive or negative. We see that in Fig. 1, the measured Seebeck coefficient S in Al at high temperatures (400 – 670 °C) is negative, while the S in noble metals (Cu, Ag, Au) are positive (Rossiter & Bass, 1994).
Based on the classical statistical idea that different temperatures generate different electron drift velocities, we obtain

$$S = -\frac{c_{\rm V}}{3ne}, \tag{1.4}$$

where $c_{\rm V}$ is the heat capacity per unit volume and n the electron density. A brief derivation of Eq. (1.4) is given in Appendix. Setting $c_{\rm V}$ equal to $3nk_{\rm B}/2$, we obtain the *classical formula* for thermopower:

$$S_{\rm classical} = -\frac{k_{\rm B}}{2e} = -0.43 \times 10^{-4}\,{\rm VK}^{-1} = -43\,\mu{\rm VK}^{-1}. \tag{1.5}$$

Observed Seebeck coefficients in metals at room temperature are of the order of microvolts per degree (see Fig. 1), a factor of 10 smaller than $S_{\rm classical}$. If we introduce the Fermi-statistically

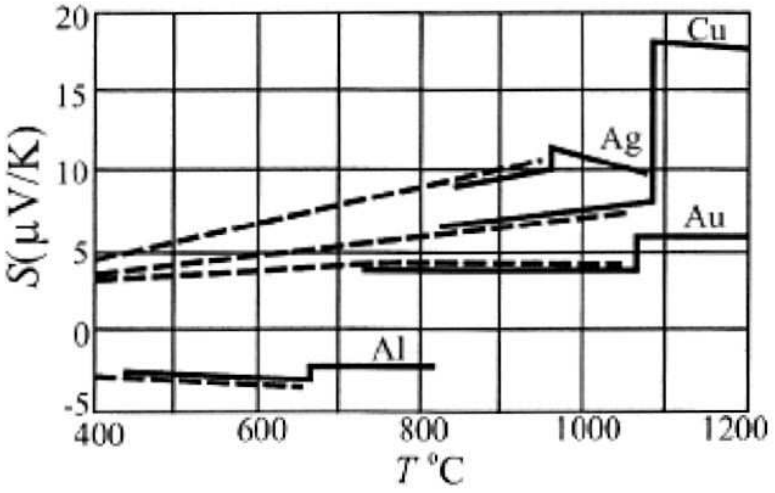

Fig. 1. High temperature Seebeck coefficients above 400 °C for Ag, Al, Au, and Cu. The solid and dashed lines represent two experimental data sets. Taken from Ref. (Rossiter & Bass, 1994).

computed specific heat

$$c_{\mathrm{V}} = \frac{1}{2}\pi^2 n k_{\mathrm{B}}(T/T_{\mathrm{F}})\,, \tag{1.6}$$

where T_{F} $(\equiv \varepsilon_{\mathrm{F}}/k_{\mathrm{B}})$ is the Fermi temperature in Eq. (1.4), we obtain

$$S_{\text{semi quantum}} = -\frac{\pi}{6}\frac{k_{\mathrm{B}}}{e}\left(\frac{k_{\mathrm{B}}T}{\varepsilon_{\mathrm{F}}}\right), \tag{1.7}$$

which is often quoted in materials handbook (Rossiter & Bass, 1994). Formula (1.7) remedies the difficulty with respect to magnitude. But the correct theory must explain the two possible signs of S besides the magnitude.
Fujita, Ho and Okamura (Fujita et al., 1989) developed a quantum theory of the Seebeck coefficient. We follow this theory and explain the sign and the T-dependence of the Seebeck coefficient. See Section 3.

2. Quantum theory

We assume that the carriers are conduction electrons ("electron", "hole") with charge q ($-e$ for "electron", $+e$ for "hole") and effective mass m^*. Assuming a one-component system, the Drude conductivity σ is given by

$$\sigma = \frac{nq^2\tau}{m^*}, \tag{2.1}$$

where n is the carrier density and τ the mean free time. Note that σ is always positive irrespective of whether $q = -e$ or $+e$. The Fermi distribution function f is

$$f(\varepsilon; T, \mu) = \frac{1}{e^{(\varepsilon-\mu)/k_{\mathrm{B}}T} + 1}, \tag{2.2}$$

where μ is the chemical potential whose value at 0 K equals the Fermi energy ε_F. The voltage difference $\Delta V = LE$, with L being the sample length, generates the chemical potential difference $\Delta\mu$, the change in f, and consequently, the electric current. Similarly, the temperature difference ΔT generates the change in f and the current.
At 0 K the Fermi surface is sharp and there are no conduction electrons. At a finite T, "electrons" ("holes") are thermally excited near the Fermi surface if the curvature of the surface is negative (positive) (see Figs. 2 and 3). We assume a high Fermi degeneracy:

$$T_F \gg T. \tag{2.3}$$

Consider first the case of "electrons". The number of thermally excited "electrons", N_x, having energies greater than the Fermi energy ε_F is defined and calculated as

$$N_x = \int_{\varepsilon_F}^{\infty} d\varepsilon \mathcal{N}(\varepsilon) \frac{1}{e^{(\varepsilon-\mu)/k_B T}+1} = \mathcal{N}_0 \int_{\varepsilon_F}^{\infty} d\varepsilon \frac{1}{e^{(\varepsilon-\mu)/k_B T}+1}$$

$$= -\mathcal{N}_0 (k_B T) \left[\ln[1+e^{-(\varepsilon-\mu)/k_B T}]\right]_{\varepsilon_F}^{\infty} \cong \ln 2 \; k_B T \mathcal{N}_0, \quad \mathcal{N}_0 = \mathcal{N}(\varepsilon_F), \tag{2.4}$$

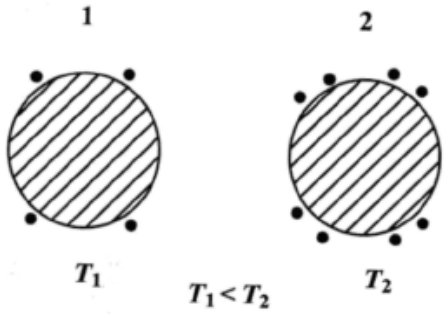

Fig. 2. More "electrons" (dots) are excited at the high temperature end: $T_2 > T_1$. "Electrons" diffuse from 2 to 1.

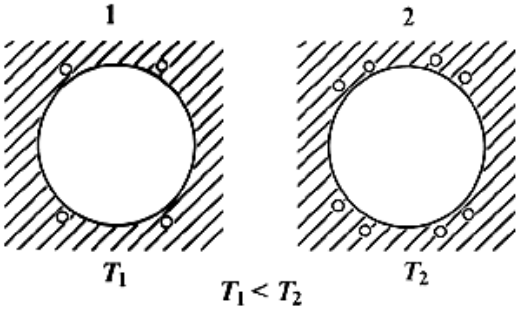

Fig. 3. More "holes" (open circles) are excited at the high temperature end: $T_2 > T_1$. "Holes" diffuse from 2 to 1.

where $\mathcal{N}(\varepsilon)$ is the density of states. The excited "electron" density $n \equiv N_x/\mathbb{V}$ is higher at the high-temperature end, and the particle current runs from the high- to the low-temperature end. This means that the electric current runs towards (away from) the high-temperature end in an "electron" ("hole")-rich material. After using Eqs. (1.3) and (2.4), we obtain

$$\begin{aligned} S < 0 \quad &\text{for} \quad \text{"electrons"}, \\ S > 0 \quad &\text{for} \quad \text{"holes"}. \end{aligned} \tag{2.5}$$

The Seebeck current arises from the thermal diffusion. We assume Fick's law:

$$\boldsymbol{j} = q\boldsymbol{j}_{\text{particle}} = -qD\boldsymbol{\nabla}n, \tag{2.6}$$

where D is the *diffusion constant*, which is computed from the standard formula:

$$D = \frac{1}{\mathrm{d}}vl = \frac{1}{\mathrm{d}}v_{\mathrm{F}}^2\tau, \quad v = v_{\mathrm{F}}, \quad l = v\tau, \tag{2.7}$$

where d is the dimension. The density gradient $\boldsymbol{\nabla}n$ is generated by the temperature gradient $\boldsymbol{\nabla}T$ and is given by

$$\boldsymbol{\nabla}n = \frac{\ln 2}{\mathbb{V}\mathrm{d}}k_{\mathrm{B}}\mathcal{N}_0\boldsymbol{\nabla}T, \tag{2.8}$$

where Eq. (2.4) is used. Using the last three equations and Eq. (1.1), we obtain

$$A = \frac{\ln 2}{\mathbb{V}}qv_{\mathrm{F}}^2k_{\mathrm{B}}\mathcal{N}_0\tau. \tag{2.9}$$

Using Eqs. (1.3), (2.1), and (2.9), we obtain

$$S = \frac{A}{\sigma} = \frac{2\ln 2}{\mathrm{d}}\left(\frac{1}{qn}\right)\varepsilon_{\mathrm{F}}k_{\mathrm{B}}\frac{\mathcal{N}_0}{\mathbb{V}}. \tag{2.10}$$

The relaxation time τ cancels out from the numerator and denominator.
The derivation of our formula [Eq. (2.10)] for the Seebeck coefficient S was based on the idea that the Seebeck emf arises from the thermal diffusion. We used the high Fermi degeneracy condition (2.3): $T_{\mathrm{F}} \gg T$. The relative errors due to this approximation *and* due to the neglect of the T-dependence of μ are both of the order $(k_{\mathrm{B}}T/\varepsilon_{\mathrm{F}})^2$. Formula (2.10) can be negative or positive, while the materials handbook formula (1.7) has the negative sign. The average speed v for highly degenerate electrons is equal to the Fermi velocity v_{F} (independent of T). Hence, semi-classical Equations (1.4) through (1.6) break down. In Ashcroft and Mermin's (AM) book (Ashcroft & Mermin, 1976), the origin of a positive S in terms of a mass tensor $M = \{m_{ij}\}$ is discussed. This tensor M is real and symmetric, and hence, it can be characterized by the principal masses $\{m_j\}$. Formula for S obtained by AM [Eq. (13.62) in Ref. (Ashcroft & Mermin, 1976)] can be positive or negative but is hard to apply in practice. In contrast our formula (2.10) can be applied straightforwardly. Besides our formula for a one-carrier system is T-independent, while the AM formula is linear in T.
Formula (2.10) is remarkably similar to the standard formula for the Hall coefficient:

$$R_{\mathrm{H}} = (qn)^{-1}. \tag{2.11}$$

Both Seebeck and Hall coefficients are inversely proportional to charge q, and hence, they give important information about the carrier charge sign. In fact the measurement of the

thermopower of a semiconductor can be used to see if the conductor is n-type or p-type (with no magnetic measurements). If only one kind of carrier exists in a conductor, then the Seebeck and Hall coefficients must have the same sign as observed in alkali metals.
Let us consider the electric current caused by a voltage difference. The current is generated by the electric force that acts on *all* electrons. The electron's response depends on its mass m^*. The density (n) dependence of σ can be understood by examining the current-carrying steady state in Fig. 4 (b). The electric field $\boldsymbol{E}$ displaces the electron distribution by a small amount $\hbar^{-1}qE\tau$ from the equilibrium distribution in Fig. 4(a). Since all the conduction electron are

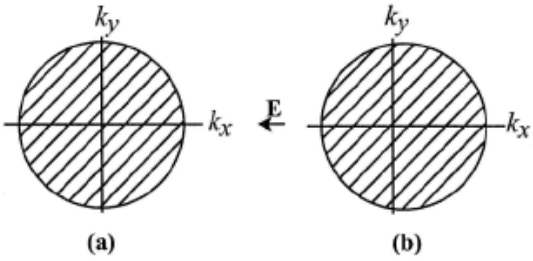

Fig. 4. Due to the electric field $\boldsymbol{E}$ pointed in the negative x-direction, the steady-state electron distribution in (b) is generated, which is a translation of the equilibrium distribution in (a) by the amount $\hbar^{-1}eE\tau$.

displaced, the conductivity σ depends on the particle density n. The Seebeck current is caused by the density difference in the thermally excited electrons near the Fermi surface, and hence, the thermal diffusion coefficient A depends on the density of states at the Fermi energy $\mathcal{N}_0$ [see Eq. (2.9)]. We further note that the diffusion coefficient D does not depend on m^* directly [see Eq. (2.7)]. Thus, the Ohmic and Seebeck currents are fundamentally different in nature.
For a single-carrier metal such as alkali metal (Na) which forms a body-centered-cubic (bcc) lattice, where only "electrons" exist, both $R_{\rm H}$ and S are negative. The *Einstein relation* between the conductivity σ and the diffusion coefficient D holds:

$$\sigma \propto D. \tag{2.12}$$

Using Eqs. (2.1) and (2.7), we obtain

$$\frac{D}{\sigma} = \frac{v_{\rm F}^2\tau/3}{q^2n\tau/m^*} = \frac{2}{3}\frac{\varepsilon_{\rm F}}{q^2n}, \tag{2.13}$$

which is a material constant. The Einstein relation is valid for a single-carrier system.

3. Applications

We consider two-carrier metals (noble metals). Noble metals including copper (Cu), silver (Ag) and gold (Au) form face-centered cubic (fcc) lattices. Each metal contains "electrons" and "holes". The Seebeck coefficient S for these metals are shown in Fig. 1. The S is positive for all

$$S > 0 \qquad \text{for Cu, Al, Ag}, \tag{3.1}$$

indicating that the majority carriers are "holes". The Hall coefficient R_H is known to be negative

$$R_H < 0 \quad \text{for Cu, Al, Ag}. \tag{3.2}$$

Clearly the Einstein relation (2.12) does not hold since the charge sign is different for S and R_H. This complication was explained by Fujita, Ho and Okamura (Fujita et al., 1989) based on the Fermi surfaces having "necks" (see Fig. 5). The curvatures along the axes of each

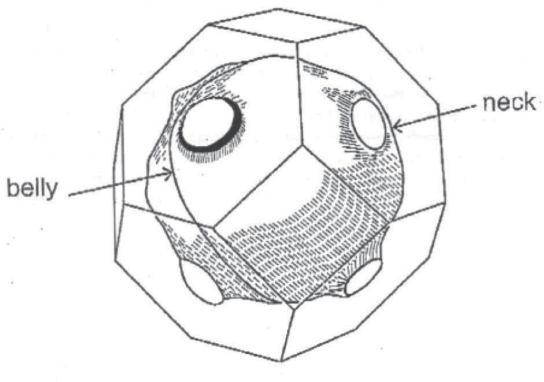

Fig. 5. The Fermi surface of silver (fcc) has "necks", with the axes in the $\langle 111 \rangle$ direction, located near the Brillouin boundary, reproduced after Ref. (Roaf, 1962; Schönberg, 1962; Schönberg & Gold, 1969).

neck are positive, and hence, the Fermi surface is "hole"-generating. Experiments (Roaf, 1962; Schönberg, 1962; Schönberg & Gold, 1969) indicate that the minimum neck area A_{111} (neck) in the k-space is 1/51 of the maximum belly area A_{111} (belly), meaning that the Fermi surface just touches the Brillouin boundary (Fig. 5 exaggerates the neck area). The density of "hole"-like states, n_{hole}, associated with the $\langle 111 \rangle$ necks, having the heavy-fermion character due to the rapidly varying surface with energy, is much greater than that of "electron"-like states, n_{electron}, associated with the $\langle 100 \rangle$ belly. The thermally excited "hole" density is higher than the "electron" density, yielding a positive S. The principal mass m_1 along the axis of a small neck ($m_1^{-1} = \partial^2 \varepsilon / \partial p_1^2$) is positive ("hole"-like) and large. The "hole" contribution to the conduction is small ($\sigma \propto m^{*-1}$), as is the "hole" contribution to Hall voltage. Then the "electrons" associated with the non-neck Fermi surface dominate and yield a negative Hall coefficient R_H.

The Einstein relation (2.12) does not hold in general for multi-carrier systems. The currents are additive. The ratio D/σ for a two-carrier system containing "electrons" (1) and "holes" (2) is given by

$$\frac{D}{\sigma} = \frac{(1/3)v_1^2\tau_1 + (1/3)v_2^2\tau_2}{q_1^2(n_1/m_1)\tau_1 + q_2^2(n_2/m_2)\tau_2}, \tag{3.3}$$

which is a complicated function of (m_1/m_2), (n_1/n_2), (v_1/v_2), and (τ_1/τ_2). In particular the mass ratio m_1/m_2 may vary significantly for a heavy fermion condition, which occurs whenever the Fermi surface just touches the Brillouin boundary. An experimental check on the violation of the Einstein relation can be be carried out by simply examining the T dependence of the ratio D/σ. This ratio D/σ depends on T since the generally T-dependent mean free times (τ_1, τ_2) arising from the electron-phonon scattering do not cancel out from

numerator and denominator. Conversely, if the Einstein relation holds for a metal, the spherical Fermi surface approximation with a single effective mass m^* is valid.
Formula (2.12) indicates that the thermal diffusion contribution to S is T-independent. The observed S in many metals is mildly T-dependent. For example, the coefficient S for Ag increases slightly before melting ($\sim$ 970 °C), while the coefficient S for Au is nearly constant and decreases, see Fig. 1. These behaviors arise from the incomplete compensation of the scattering effects. "Electrons" and "holes" that are generated from the complicated Fermi surfaces will have different effective masses and densities, and the resulting incomplete compensation of τ's (*i.e.*, the scattering effects) yields a T-dependence.

4. Graphene and carbon nanotubes

4.1 Introduction

Graphite and diamond are both made of carbons. They have different lattice structures and different properties. Diamond is brilliant and it is an insulator while graphite is black and is a good conductor. In 1991 Iijima (Iijima, 1991) discovered carbon nanotubes (graphite tubules) in the soot created in an electric discharge between two carbon electrodes. These nanotubes ranging 4 to 30 nanometers (nm) in diameter are found to have helical multi-walled structure as shown in Figs. 6 and 7 after the electron diffraction analysis. The tube length is about one micrometer (μm).

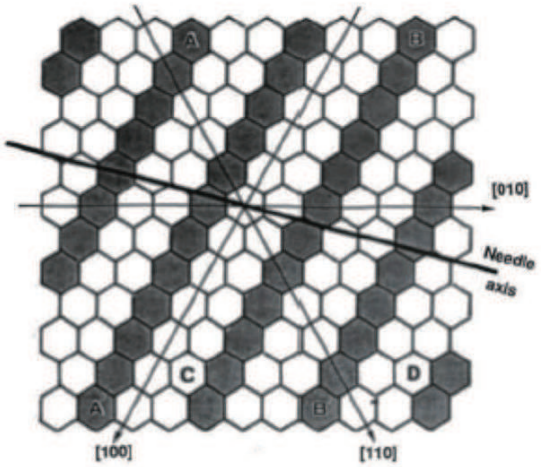

Fig. 6. Schematic diagram showing a helical arrangement of a carbon nanotube, unrolled (reproduced from Ref. (Iijima, 1991)). The tube axis is indicated by the heavy line and the hexagons labelled A and B, and A′ and B′, are superimposed to form the tube. The number of hexagons does not represent a real tube size.

The scroll-type tube shown in Fig. 7 is called the *multi-walled carbon nanotube* (MWNT). *Single-walled nanotube* (SWNT) shown in Fig. 8 was fabricated by Iijima and Ichihashi (Iijima & Ichihashi, 1993) and by Bethune *et al*. (Bethune et al., 1993). The tube size

is about one nanometer in diameter and a few microns (μ) in length. The tube ends are closed as shown in Fig. 8. Unrolled carbon sheets are called *graphene*. They have honeycomb lattice structure as shown in Figs. 6 and 9. Carbon nanotubes are light since they are entirely made of light element carbon (C). They are strong and have excellent elasticity and flexibility. In fact, carbon fibers are used to make tennis rackets, for example. Today's semiconductor technology is based mainly on silicon (Si). It is said that carbon devices are expected to be as important or even more important in the future. To achieve this we must know the electrical transport properties of carbon nanotubes.

In 2003 Kang *et al.* (Kang et al., 2003) reported a logarithmic temperature (T) dependence of the Seebeck coefficient S in multiwalled carbon nanotubes at low temperatures ($T = 1.5$ K). Their data are reproduced in Fig. 10, where S/T is plotted on a logarithmic temperature scale after Ref. (Kang et al., 2003), Fig. 2. There are clear breaks in data around $T_0 = 20$ K. Above this temperature T_0, the Seebeck coefficient S is linear in temperature T:

$$S = aT\,, \qquad T > T_0 = 20\,\mathrm{K} \tag{4.1}$$

where $a = 0.15\ \mu\mathrm{V/K}^2$. Below 20 K the temperature behavior is approximately

$$S \sim T \ln T, \qquad T < T_0\,. \tag{4.2}$$

The original authors (Kang et al., 2003) regarded the unusual behavior (4.2) as the intrinsic behavior of MWNT, arising from the combined effects of electron-electron interaction and

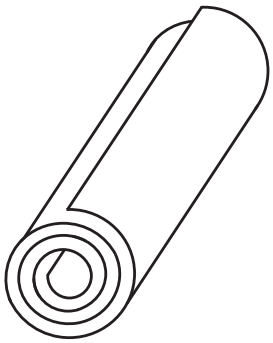

Fig. 7. A model of a scroll-type filament for a multi-walled nanotube.

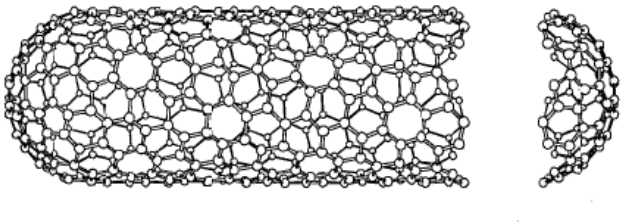

Fig. 8. Structure of a single-walled nanotube (SWNT) (reproduced from Ref. (Saito et al., 1992)). Carbon pentagons appear near the ends of the tube.

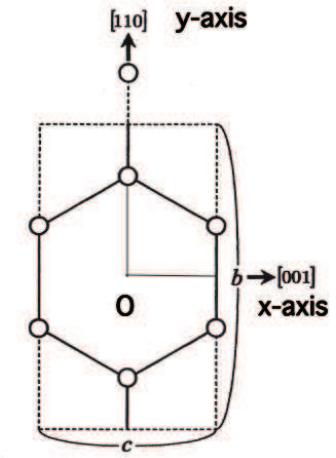

Fig. 9. A rectangular unit cell of graphene. The unit cell contains four C (open circle).

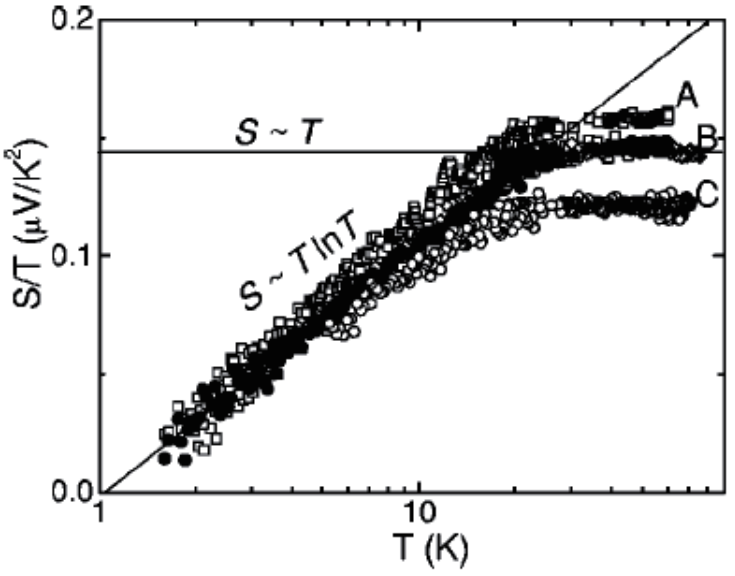

Fig. 10. A logarithmic temperature (T) dependence of the Seebeck coefficient S in MWNT after Ref. (Kang et al., 2003). A, B and C are three samples with different doping levels.

electron-disorder scattering. The effects are sometimes called as two-dimensional weak localization (2D WL) (Kane & Fisher, 1992; Langer et al., 1996). Their interpretation is based on the electron-carrier transport. We propose a different interpretation. Both (4.1) and (4.2) can be explained based on the Cooper-pairs (pairons) carrier transport. The pairons are generated by the phonon exchange attraction. We shall show that the pairons generate the T-linear behavior in (4.1) above the superconducting temperature T_0 *and* the $T \ln T$ behavior in (4.2) below T_0.

The current band theory of the honeycomb crystal based on the Wigner-Seitz (WS) cell model (Saito et al., 1998; Wigner & Seitz, 1933) predicts a gapless semiconductor for graphene, which is not experimentally observed. The WS model (Wigner & Seitz, 1933) was developed for the study of the ground-state energy of the crystal. To describe the Bloch electron motion in terms of the mass tensor (Ashcroft & Mermin, 1976) a new theory based on the Cartesian unit cell not matching with the natural triangular crystal axes is necessary. Only then, we can discuss the anisotropic mass tensor. Also phonon motion can be discussed, using Cartesian coordinate-systems, not with the triangular coordinate systems. The conduction electron moves as a wave packet formed by the Bloch waves as pointed out by Ashcroft and Mermin in their book (Ashcroft & Mermin, 1976). This picture is fully incorporated in our new theoretical model. We discuss the Fermi surface of graphene in section 4.2.

4.2 The Fermi surface of graphene

We consider a graphene which forms a two-dimensional (2D) honeycomb lattice. The normal carriers in the electrical charge transport are "electrons" and "holes." The "electron" ("hole") is a quasi-electron that has an energy higher (lower) than the Fermi energy *and* which circulates counterclockwise (clockwise) viewed from the tip of the applied magnetic field vector. "Electrons" ("holes") are excited on the positive (negative) side of the Fermi surface with the convention that the positive normal vector at the surface points in the energy-increasing direction.

We assume that the "electron" ("hole") wave packet has the charge $-e$ $(+e)$ and a size of a unit carbon hexagon, generated above (below) the Fermi energy ε_F. We will show that (a) the "electron" and "hole" have different charge distributions and different effective masses, (b) that the "electrons" and "holes" are thermally activated with different energy gaps $(\varepsilon_1, \varepsilon_2)$, and (c) that the "electrons" and "holes" move in different easy channels.

The positively-charged "hole" tends to stay away from positive ions C^+, and hence its charge is concentrated at the center of the hexagon. The negatively charged "electron" tends to stay close to the C^+ hexagon and its charge is concentrated near the C^+ hexagon. In our model, the "electron" and "hole" both have charge distributions, and they are not point particles. Hence, their masses m_1 and m_2 must be different from the gravitational mass $m = 9.11 \times 10^{-28}$ g. Because of the different internal charge distributions, the "electrons" and "holes" have the different effective masses m_1 and m_2. The "electron" may move easily with a smaller effective mass in the direction [110 c-axis]$\equiv$ [110] than perpendicular to it as we see presently. Here, we use the conventional Miller indices for the hexagonal lattice with omission of the c-axis index. For the description of the electron motion in terms of the mass tensor, it is necessary to introduce Cartesian coordinates, which do not necessarily match with the crystal's natural (triangular) axes. We may choose the rectangular unit cell with the side-length pair (b, c) as shown in Fig. 9. Then, the Brillouin zone boundary in the k space is unique: a rectangle with side lengths $(2\pi/b, 2\pi/c)$. The "electron" (wave packet) may move up or down in [110] to the neighboring hexagon sites passing over one C^+. The positively charged C^+ acts as a

welcoming (favorable) potential valley center for the negatively charged "electron" while the same C^+ acts as a hindering potential hill for the positively charged "hole". The "hole" can however move easily over on a series of vacant sites, each surrounded by six C^+, without meeting the hindering potential hills. Then, the easy channel directions for the "electrons" and "holes" are [110] and [001], respectively.

Let us consider the system (graphene) at 0 K. If we put an electron in the crystal, then the electron should occupy the center O of the Brillouin zone, where the lowest energy lies. Additional electrons occupy points neighboring O in consideration of Pauli's exclusion principle. The electron distribution is lattice-periodic over the entire crystal in accordance with the Bloch theorem. The uppermost partially filled bands are important for the transport properties discussion. We consider such a band. The 2D Fermi surface which defines the boundary between the filled and unfilled k-space (area) is *not* a circle since the x-y symmetry is broken. The "electron" effective mass is smaller in the direction [110] than perpendicular to it. That is, the "electron" has two effective masses and it is intrinsically anisotropic. If the "electron" number is raised by the gate voltage, then the Fermi surface more quickly grows in the easy-axis (y) direction, say [110] than in the x-direction, i.e., [001]. The Fermi surface must approach the Brillouin boundary at right angles because of the inversion symmetry possessed by the honeycomb lattice. Then at a certain voltage, a "neck" Fermi surface must be developed.

The same easy channels in which the "electron" runs with a small mass, may be assumed for other hexagonal directions, [011] and [101]. The currents run in three channels $\langle 110\rangle \equiv [110]$, [011], and [101]. The electric field component along a channel j is reduced by the directional cosine $\cos(\mu, j)$ $(= \cos\vartheta)$ between the field direction μ and the channel direction j. The current is reduced by the same factor in the Ohmic conduction. The total current is the sum of the channel currents. Then its component along the field direction is proportional to

$$\sum_{j\,\text{channel}} \cos^2(\mu, j) = \cos^2\vartheta + \cos^2(\vartheta + 2\pi/3) + \cos^2(\vartheta - 2\pi/3) = 3/2\,. \tag{4.3}$$

There is no angle (ϑ) dependence. The current is isotropic. The number $3/2$ represents the fact that the current density is higher by this factor for a honeycomb lattice than for the square lattice.

We have seen that the "electron" and "hole" have different internal charge distributions and they therefore have different effective masses. Which carriers are easier to be activated or excited? The "electron" is near the positive ions and the "hole" is farther away from the ions. Hence, the gain in the Coulomb interaction is greater for the "electron." That is, the "electron" are more easily activated (or excited). The "electron" move in the welcoming potential-well channels while the "hole" do not. This fact also leads to the smaller activation energy for the electrons. We may represent the activation energy difference by

$$\varepsilon_1 < \varepsilon_2\,. \tag{4.4}$$

The thermally activated (or excited) electron densities are given by

$$n_j(T) = n_j e^{-\varepsilon_j/k_B T}\,, \tag{4.5}$$

where $j = 1$ and 2 represent the "electron" and "hole", respectively. The prefactor n_j is the density at the high temperature limit.

4.3 Single-walled nanotubes (SWNT)

Let us consider a long SWNT rolled with the graphene sheet. The charge may be transported by the channeling "electrons" and "holes" in the graphene wall. But the "holes" present inside the SWNT can also contribute to the charge transport. The carbon ions in the wall are positively charged. Hence, the positively charged "hole" can go through inside tube. In contrast, the negatively charged "electrons" are attracted by the carbon wall and cannot go straight in the tube. Because of this extra channel inside the carbon nanotube, "holes" can be the majority carriers in nanotubes although "electrons" are the dominant carriers in graphene. Moriyama *et al.* (Moriyama et al., 2004) observed the electrical transport in SWNT in the temperature range 2.6 - 200 K, and found from the field effect (gate voltage) study that the carriers are "holes".

The conductivity was found to depend on the pitch of the SWNT. The helical line is defined as the line in $\langle 100 \rangle$ passing the centers of the nearest neighbors of the C^+ hexagons. The helical angle φ is the angle between the helical line and the tube axis. The degree of helicity h may be defined as

$$h = \cos\varphi\,. \tag{4.6}$$

For a macroscopically large graphene the conductivity does not show any directional dependence (Fujita & Suzuki, 2010) as we saw in Sec. 4.2. The electrical conduction in SWNT depends on the pitch (Dai et al., 1996; Ebbesen et al., 1996) and can be classified into two groups: either semiconducting or metallic (Saito et al., 1998; Tans et al., 1997). This division in two groups arises as follows. A SWNT is likely to have an integral number of carbon hexagons around the circumference. If each pitch contains an integral number of hexagons, then the system is periodic along the tube axis, and "holes" (not "electrons") can move along the tube. Such a system is semiconducting and the electrical conduction is then characterized by an activation energy ε_2. The energy ε_2 has distribution since both the pitch and circumference have distributions. The pitch angle is not controlled in the fabrication processes. There are, then, more numerous cases where the pitch contains an irrational numbers of hexagons. In these cases the system shows a metallic behavior experimentally observed (Tans et al., 1998).

4.4 Multi-walled nanotubes (MWNT)

MWNT are open-ended. Hence, each pitch is likely to contain an irrational number of carbon hexagons. Then, the electrical conduction of MWNT is similar to that of metallic SWNT. The conductivity σ based on the pairon carrier model is calcullated as follows.

The pairons move in 2D with the linear dispersion relation (Fujita et al., 2009):

$$\varepsilon_{\rm p} = c^{(j)} p, \tag{4.7}$$

$$c^{(j)} = (2/\pi) v_{\rm F}^{(j)}\,, \tag{4.8}$$

where $v_{\rm F}^{(j)}$ is the Fermi velocity of the "electron" $(j = 1)$ ["hole" $(j = 2)$].

Consider first "electron"-pairs. The velocity $\boldsymbol{v}$ is given by (omitting superscript)

$$\boldsymbol{v} = \frac{\partial \varepsilon_{\rm p}}{\partial \boldsymbol{p}} \quad \text{or} \quad v_x = \frac{\partial \varepsilon_{\rm p}}{\partial p}\frac{\partial p}{\partial p_x} = c\frac{p_x}{p}\,, \tag{4.9}$$

where we used Eq. (4.7) for the pairon energy $\varepsilon_{\rm p}$ and the 2D momentum,

$$p \equiv (p_x^2 + p_y^2)^{1/2}\,. \tag{4.10}$$

The equation of motion along the electric field E in the x-direction is

$$\frac{\partial p_x}{\partial t} = q' E \,, \tag{4.11}$$

where q' is the charge $\pm 2e$ of a pairon. The solution of Eq. (4.11) is given by

$$p_x = q' E t + p_x^{(0)} \,, \tag{4.12}$$

where $p_x^{(0)}$ is the initial momentum component. The current density $j_{\rm p}$ is calculated from (charge q') $\times$ (number density $n_{\rm p}$) $\times$ (average velocity $\bar{v}$). The average velocity $\bar{v}$ is calculated by using Eq. (4.9) and Eq. (4.12) with the assumption that the pair is accelerated only for the collision time τ *and* the initial-momentum-dependent terms are averaged out to zero. We then obtain

$$j_{\rm p} = q' n_{\rm p} \bar{v} = q' n_{\rm p} c \frac{\bar{p}_x}{p} = q'^2 n_{\rm p} \frac{c}{p} E \tau \,. \tag{4.13}$$

For stationary currents, the partial pairon density $n_{\rm p}$ is given by the Bose distribution function $f(\varepsilon_{\rm p})$:

$$n_{\rm p} = f(\varepsilon_{\rm p}) \equiv [\exp(\varepsilon_{\rm p}/k_{\rm B}T - \alpha) - 1]^{-1} \,, \tag{4.14}$$

where e^{α} is the fugacity. Integrating the current $j_{\rm p}$ over all 2D p-space, and using Ohm's law $j = \sigma E$, we obtain for the conductivity σ:

$$\sigma = (2\pi\hbar)^{-2} q'^2 c \int {\rm d}^2 p \, p^{-1} f(\varepsilon_{\rm p}) \tau \,. \tag{4.15}$$

In the low temperatures we may assume the Boltzmann distribution function for $f(\varepsilon_{\rm p})$:

$$f(\varepsilon_{\rm p}) \simeq \exp(\alpha - \varepsilon_{\rm p}/k_{\rm B}T) \,. \tag{4.16}$$

We assume that the relaxation time arises from the phonon scattering so that

$$\tau = (aT)^{-1} \,, \quad a = \text{constant.} \tag{4.17}$$

After performing the p-integration we obtain from Eq. (4.15)

$$\sigma = \frac{2}{\pi} \frac{e^2 k_{\rm B}}{a\hbar^2} e^{\alpha} \,, \tag{4.18}$$

which is temperature-independent. If there are "electrons" and "hole" pairons, they contribute additively to the conductivity. These pairons should undergo a Bose-Einstein condensation at lowest temperatures.

We are now ready to discuss the Seebeck coefficient S of MWNT. First, we will show that the S is proportional to the temperature T above the superconducting temperature T_0.

We start with the standard formula for the charge current density:

$$\boldsymbol{j} = q' n \bar{\boldsymbol{v}} \,, \tag{4.19}$$

where $\bar{\boldsymbol{v}}$ is the average velocity, which is a function of temperature T and the particle density n:

$$\bar{\boldsymbol{v}} = \boldsymbol{v}(n, T) \,. \tag{4.20}$$

We assume a steady state in which the temperature T varies only in the x-direction while the density is kept constant. The temperature gradient $\partial T/\partial x$ generates a current:

$$j = q' n \frac{\partial v(n,T)}{\partial T} \frac{\partial T}{\partial x} \Delta x \,. \tag{4.21}$$

The thermal diffusion occurs locally. We may choose Δx to be a mean free path:

$$\Delta x = l = v\tau \,. \tag{4.22}$$

The current coming from the 2D pairon momentum $\boldsymbol{p}$, which is generated by the temperature gradient $\partial T/\partial x$, is thus given by

$$j_{\rm p} = q' n_{\rm p} \bar{v}_x(n_{\rm p}, T) = q' n_{\rm p} \frac{\partial v}{\partial T} \frac{\partial T}{\partial x} v\tau \,. \tag{4.23}$$

Integrating Eq. (4.23) over all 2D p-space and comparing with Eq. (1.1), we obtain

$$A = (2\pi\hbar)^{-2} q' \frac{\partial v}{\partial T} \int {\rm d}^2 p v_x f(\varepsilon_{\rm p}) \tau$$

$$= (2\pi\hbar)^{-2} q' \frac{\partial v}{\partial T}\, c \int {\rm d}^2 p \frac{p_x}{p} f(\varepsilon_{\rm p}) \tau \,. \tag{4.24}$$

We compare this integral with the integral in Eq. (4.15). It has an extra factor in p and generates therefore an extra factor T when the Boltzmann distribution function is adopted for $f(\varepsilon_{\rm p})$. Thus, we obtain

$$S = \frac{A}{\sigma} \propto T \,. \tag{4.25}$$

We next consider the system below the superconducting temperature T_0. The supercurrents arising from the condensed pairons generate no thermal diffusion. But non-condensed pairons can be scattered by impurities and phonons, and contribute to a thermal diffusion. Because of the zero-temperature energy gap

$$\varepsilon_{\rm g} \equiv k_{\rm B} T_{\rm g} \tag{4.26}$$

generated by the supercondensate, the population of the non-condensed pairons is reduced by the Boltzmann-Arrhenius factor

$$\exp(-\varepsilon_{\rm g}/k_{\rm B}T) = \exp(-T_{\rm g}/T) \,. \tag{4.27}$$

This reduction applies only for the conductivity (and not for the diffusion). Hence we obtain the Seebeck coefficient:

$$\frac{A}{\sigma} \propto \frac{T}{\exp(-T_{\rm g}/T)} = T \exp(T_{\rm g}/T) \,. \tag{4.28}$$

In the experiment MWNT bundles containing hundreds of individual nanotubes are used. Both circumference and pitch have distributions. Hence, the effective energy gap temperature $T_{\rm g}$ has a distribution. We may then replace (Jang et al., 2004)

$$\exp(T_{\rm g}/T) \quad \text{by} \quad (T'_{\rm g}/T)^{1/3} \tag{4.29}$$

where T'_g is a temperature of the order T_g. We then obtain

$$\frac{A}{\sigma} \propto T(T'_g/T)^{1/3}. \tag{4.30}$$

In summary, by considering moving pairons we obtained the T-linear behavior of the Seebeck coefficient S above the superconducting temperature T_c and the $T \ln T$-behavior of S at the lowest temperatures. The energy gap ε_g vanishes at T_c. Hence, the temperature behaviors should be smooth and monotonic as observed in Fig. 10. This supports the present interpretation based on the superconducting phase transition. The doping changes the pairon density and the superconducting temperature. Hence the data for A, B and C in Fig. 10 are reasonable.

Based on the idea that different temperatures generate different carrier densities and the resulting carrier diffusion generates a thermal electromotive force (emf), we obtained a new formula for the Seebeck coefficient (thermopower) S:

$$S = \frac{2\ln 2}{\mathrm{d}} \frac{1}{qn} \varepsilon_F k_B \frac{\mathcal{N}_0}{\mathbb{V}},$$

where k_B is the Boltzmann constant, d the dimension, q, n, ε_F, $\mathcal{N}_0$ and $\mathbb{V}$ are charge, carrier density, Fermi energy, density of states at ε_F, and volume, respectively. Ohmic and Seebeck currents are fundamentally different in nature, and hence, cause significantly different transport behaviors. For example, the Seebeck coefficient S in copper (Cu) is positive, while the Hall coefficient is negative. In general, the Einstein relation between the conductivity and the diffusion coefficient does not hold for a multicarrier metal. Multi-walled carbon nanotubes are superconductors. The Seebeck coefficient S is shown to be proportional to the temperature T above the superconducting temperature T_0 based on the model of Cooper pairs as carriers. The S below T_0 follows a temperature behavior, $S/T \propto (T'_g/T)^{1/3}$, where T'_g = constant, at the lowest temperatures.

5. Appendix: Derivation of Eq. (1.4)

In order to clearly understand diffusion let us look at the following simple situation. Imagine that four particles are in space a, and two particles are in space b as shown in Fig. 11. Assuming that both spaces a and b have the same volume, we may say that the particle density is higher in a than in b. We assume that half of the particles in each space will be heading toward the boundary CC′. It is then natural to expect that in due time two particles would cross the boundary CC′ from a to b, and one particle from b to a. This means that more particles would pass the boundary from a to b, that is, from the side of high density to that of low density. This is, in fact, the cause of diffusion.

The essential points in the above arguments are the reasonable assumptions that

(a) the particles flow out from a given space in all directions with the *same* probability, and

(b) the rate of this outflow is proportional to the number of particles contained in that space.

In the present case the condition (a) will be assured by the fact that each electron *collides* with impurities frequently so that it may lose the memory of how it entered the space originally and may leave with *no* preferred direction. In a more quantitative study it is found that the particle current $\boldsymbol{j}$ is proportional to the density gradient $\boldsymbol{\nabla} n$:

$$\boldsymbol{j} = -D\boldsymbol{\nabla} n, \tag{A.1}$$

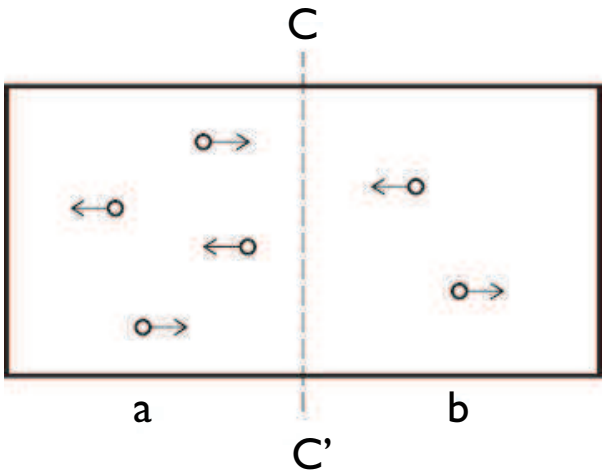

Fig. 11. If the particles flow out in all directions with no preference, there will be more particles crossing the imaginary boundary CC′ in the a to b direction than in the opposite direction.

where D is the diffusion coefficient. This linear relation (A.1) is called *Fick's law*.
Consider next *thermal conduction*. Assume that the spaces a and b are occupied by the same numbers of the particles. Further assume that the temperature T is higher in b than in a. Then, the particle speed is higher in b than in a in the average. In due time a particle crosses the boundary CC′ from a to b and another crosses the boundary CC′ from b to a. Then, the energy is transferred through the boundary. In a more detailed study *Fourier's law* is observed:

$$\boldsymbol{q} = -K\boldsymbol{\nabla}T\,, \tag{A.2}$$

where $\boldsymbol{q}$ is the heat (energy) current and K is called the *thermal conductivity*.
We now take a system of free electrons with mass m and charge $-e$ immersed in a uniform distribution of impurities which act as scatterers. We assume that a free classical electron system in equilibrium is characterized by the ideal gas condition so that the average electron energy ε depends on the temperature T only:

$$\varepsilon = \varepsilon(n, T) = \varepsilon(T)\,, \tag{A.3}$$

where n is the electron density. The electric current density $\boldsymbol{j}$ is given by

$$\boldsymbol{j} = (-e)n\boldsymbol{v}\,, \tag{A.4}$$

where $\boldsymbol{v}$ is the velocity field (average velocity). We assume that the density n is constant in space and time. If there is a temperature gradient, then there will be a current as shown below. We assume first a one-dimensional (1D) motion. The velocity field v depends on the temperature T, which varies in space.
Assume that the temperature T is higher at $x + \Delta x$ than at x:

$$T(x + \Delta x) > T(x)\,. \tag{A.5}$$

Then

$$v[n, T(x+\Delta x)] - v[n, T(x)] = \frac{\partial v(n,T)}{\partial T}\frac{\partial T}{\partial x}\Delta x\,. \tag{A.6}$$

The diffusion and heat conduction occur locally. We may choose Δx to be a mean free path

$$l = v\tau\,, \tag{A.7}$$

which is constant in our system. Then the current j is, from Eq. (A.4),

$$j = (-e)n\frac{\partial v}{\partial T}l\frac{\partial T}{\partial x}\,. \tag{A.8}$$

Using Eqs. (1.1), (A.7) and (A.8), we obtain

$$A = (-e)n\frac{\partial v}{\partial T}v\tau\,. \tag{A.9}$$

The conductivity σ is given by the Drude formula:

$$\sigma = e^2\frac{n}{m}\tau\,. \tag{A.10}$$

Thus, the Seebeck coefficient S is, using Eqs. (A.9) and (A.10),

$$\begin{aligned} S = \frac{A}{\sigma} &= -\frac{1}{ne}m\frac{\partial v}{\partial T}\frac{l}{\tau} = -\frac{1}{ne}m\frac{\partial v^2}{\partial T} \\ &= -\frac{1}{ne}\frac{\partial}{\partial T}\left(\frac{1}{2}mv^2\right) = -\frac{1}{ne}\frac{\partial \varepsilon}{\partial T} = -\frac{1}{ne}c\,, \end{aligned} \tag{A.11}$$

where

$$c \equiv \frac{\partial \varepsilon}{\partial T}\,. \tag{A.12}$$

is the heat capacity per electron.
Our theory can simply be extended to a 3D motion. The equipartition theorem holds for the classical electrons:

$$\left\langle \frac{1}{2}mv_x^2 \right\rangle = \left\langle \frac{1}{2}mv_y^2 \right\rangle = \left\langle \frac{1}{2}mv_z^2 \right\rangle = \frac{1}{2}k_{\mathrm{B}}T\,, \tag{A.13}$$

where the angular brackets mean the equilibrium average. Hence the average energy is

$$\varepsilon \equiv \frac{1}{2}mv^2 = \frac{1}{2}(v_x^2 + v_y^2 + v_z^2) = \frac{3}{2}k_{\mathrm{B}}T\,. \tag{A.14}$$

We obtain

$$A = -en\frac{1}{2}\frac{\partial v^2}{\partial t}\tau\,. \tag{A.15}$$

Using this, we obtain the Seebeck coefficient for a 3D motion as

$$S = \frac{A}{\sigma} = -\frac{c_{\mathbb{V}}}{3ne} = -\frac{k_{\mathrm{B}}}{2e}\,, \tag{A.16}$$

where

$$c_{\mathbb{V}} \equiv \frac{\partial \varepsilon}{\partial T} = \frac{3}{2}k_{\mathrm{B}} \tag{A.17}$$

is the heat capacity per electron. The heat capacity per unit volume, $c_{\mathbb{V}}$, is related by the heat capacity per electron, c, by

$$c_{\mathbb{V}} = nc\,. \tag{A.18}$$

6. References

Ashcroft, N. W. & Mermin, N. D. (1976). *Solid State Physics* (Saunders, Philadelphia), pp. 256–258, 290–293.

Bethune, D. S., Kiang, C. H., de Vries, M. S., Gorman, G., Savoy, R., Vazquez, J. & Beyers, R. (1993). Cobalt-catalysed growth of carbon nanotubes with single-atomic-layer walls, *Nature* Vol. 363, 605–607.

Dai. H., Wong, E. W. & Lieber, C. M. (1996). Probing Electrical Transport in Nanomaterials: Conductivity of individual Carbon Nanotubes, *Science* Vol. 272, 523–526.

Ebbesen, T. W., Lezec. H. J., Hiura, H., Bennett, J. W., Ghaemi, L. J. & Thio, T. (1996). Electrical conductivity of individual carbon nanotubes, *Nature* Vol. 382, 54–56.

Fujita, S., Ho, H-C. & Okamura, Y. (2000). Quantum Theory of the Seebeck Coefficient in Metals, *Int. J. Mod. Phys.* B Vol. 14, 2231–2240.

Fujita, S., Ito, K. & Godoy, S. (2009). *Quantum Theory of Conducting Matter. Superconductivity* (Springer, New York) pp. 77–79.

Fujita, S. & Suzuki, A. (2010). Theory of temperature dependence of the conductivity in carbon nanotubes, *J. Appl. Phys.* Vol. 107, 013711–4.

Iijima, S. (1991). Helical microtubules of graphitic carbon, *Nature* Vol. 354. 56–58.

Iijima, S. & Ichihashi, T. (1993). Single-shell carbon nanotubes of 1-nm diameter, *Nature* Vol. 363, 603–605.

Jang, W. Y., Kulkami, N. N., Shih, C. K. & Yao, Z. (2004). Electrical characterization of individual carbon nanotubes grown in nano porous anodic alumina templates, *Appl. Phys. Lett.* Vol. 84, 1177–1180.

Kane, C. L. & Fisher, M. P. A. (1992). Transport in a one-channel Luttinger liquid, *Phys. Rev. Lett.* Vol. 68, 1220–1223.

Kang, N, Lu, L., Kong, W. J., Hu, J. S., Yi, W., Wang, Y. P., Zhang, D. L., Pan, Z. W & Xie, S. S. (2003). Observation of a logarithmic temperature dependence of thermoelectric power in multi wall carbon nanotubes, *Phys. Rev.* B Vol. 67, 033404–4.

Langer, L., *et al.* (1996). Quantum Transport in a Multiwalled Carbon Nanotube, *Phys. Rev. Lett.* Vol. 76, 479–482.

Moriyama, S., Toratani, K., Tsuya, D., Suzuki, M. Aoyagi, Y. & Ishibashi, K. (2004). Electrical transport in semiconducting carbon nanotubes, *Physica* E Vol. 24, 46–49.

Roaf, D. J. (1962). The Fermi Surface of Copper, Silver and Gold II. Calculation of the Fermi Surfaces, *Phil. Trans. R. Soc. Lond.* Vol. 255, 135–152.

Rossiter, P. L. & Bass, J. (1994). *Metals and Alloys*. in *Encyclopedia of Applied Physics* 10, (Wiley-VCH Publ., Berlin), pp. 163–197.

Saito, R., Fujita, M., Dresselhaus, G. & Dresselhaus, M. S. (1992). Electronic structure of chiral graphene tubles, *Appl. Phys. Lett.* Vol. 60, 2204–2206.

Saito, R.; Dresselhaus, G. & Dresselhaus, M. S. (1998). *Physical Properties of Carbon Nanotubes* (Imperial College, London) pp. 156–157.

Schönberg, D. (1962). The Fermi Surfaces of Copper, Silver and Gold I. The de Haas-van Alphen Effect, *Phil. Trans. R. Soc. Lond.* Vol. 255, 85–133.

Schönberg, D. & Gold, A. V. (1969). *Physics of Metals-1*, in *Electrons*, ed. Ziman, J. M. (Cambridge University Press, UK), p. 112.

Tans, S. J., Devoret, M. H., Dai, H., Thess, A., Smalley, R., Geerligs, L. J. & Dekker. C. (1997). Individual single-wall carbon nanotubes as quantum wires, *Nature* Vol. 386, 474–477.

Tans, S. J., Vershueren, A. R. M. & Dekker, C. (1998). Room-temperature transistor based on a single carbon nanotube, *Nature* Vol. 393, 49–52.

Wigner, E. & Seitz, F. (1933), On the Constitution of Metallic Sodium, *Phys. Rev.* Vol. 43, 804–810.

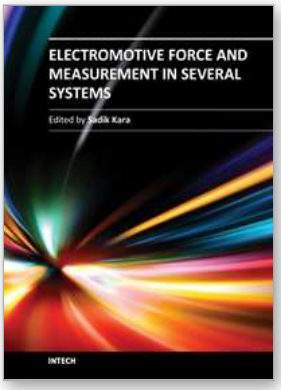

Electromotive Force and Measurement in Several Systems
Edited by Prof. Sadik Kara

ISBN 978-953-307-728-4
Hard cover, 174 pages
Publisher InTech
Published online 21, November, 2011
Published in print edition November, 2011

This book is devoted to different sides of Electromotive Force theory and its applications in Engineering science and Industry. The covered topics include the Quantum Theory of Thermoelectric Power (Seebeck Coefficient), Electromotive forces in solar energy and photocatalysis (photo electromotive forces), Electromotive Force in Electrochemical Modification of Mudstone, The EMF method with solid-state electrolyte in the thermodynamic investigation of ternary copper and silver chalcogenides, Electromotive Force Measurements and Thermodynamic Modelling of Electrolyte in Mixed Solvents, Application of Electromotive Force Measurement in Nuclear Systems Using Lead Alloys, Electromotive Force Measurements in High-Temperature Systems and finally, Resonance Analysis of Induced EMF on Coils.

INTECH
open science | open minds

InTech Europe
University Campus STeP Ri
Slavka Krautzeka 83/A
51000 Rijeka, Croatia
Phone: +385 (51) 770 447
Fax: +385 (51) 686 166
www.intechopen.com

InTech China
Unit 405, Office Block, Hotel Equatorial Shanghai
No.65, Yan An Road (West), Shanghai, 200040, China
中国上海市延安西路65号上海国际贵都大饭店办公楼405单元
Phone: +86-21-62489820
Fax: +86-21-62489821